

Accuracy of Disk Method to Predict Roll Residual Stress by Measuring the Sliced Disk Stress

Nao-Aki NODA,* Kejun HU, Yoshikazu SANNO, Yusuke HOSOKAWA and Xu WANG

Department of Mechanical Engineering, Kyushu Institute of Technology, 1-1 Sensui-cho, Tobata-ku, Kitakyushu-shi, Fukuoka, 804-8550 Japan.

(Received on November 4, 2016; accepted on April 13, 2017)

Bimetallic rolls are widely used in steel rolling industries because of the excellent hardness, wear resistance and high temperature properties. Controlling the residual stress distribution is necessary since the compressive residual stress at the surface may improve fatigue life though the tensile residual stress at the center may reduce the strength. Therefore, it is necessary to measure the residual stress distribution from the surface to center correctly to ensure the roll quality. The disk method has been widely used in predicting the roll residual stress by measuring the stress of the thin sliced disk from the roll. In this study, therefore, the relation between the original roll residual stress and the sliced disk residual stress is investigated for the single material roll and bimetallic roll on the basis of thermo-elastic-plastic FEM analysis. The effect of the quenching time is discussed as well as the effect of the sliced disk thickness on the residual stress.

KEY WORDS: residual stress; FEM simulation; rolling; disk method; heat treatment.

1. Introduction

Work rolls are widely used in the roughing stands of hot strip mill to reduce steel thickness. During hot rolling process, thermal stresses are caused by a cyclic sequence of heating and cooling over the roll surface. Due to hot strip contact and water cooling, thermal cracks named firecracks initiate at the roll surface.¹⁻⁴⁾ If severe thermal tensile stress is added under some rolling troubles, thermal crack starts propagating. Therefore, a suitable compressive stress is necessary for preventing thermal crack extension.⁵⁾ However, a tensile residual stress always appears at the roll center to balance the surface compressive residual stress. Under the combined action of thermal stress and residual stress, another form of roll fracture is known as thermal barrel breakage as shown in **Fig. 1**. This thermal breakage originates near the roll center and breaks out to the barrel surface.⁶⁻⁸⁾ In our previous studies,^{9,10)} therefore, different quenching methods were discussed through FEM simulation to produce suitable surface compressive residual stresses and reduce the center tensile residual stress. In real work rolls, however, the existence of suitable residual stress distribution should be confirmed experimentally.

Over the years, different measuring methods have been developed for work rolls in order to confirm the roll residual stress distribution. Those methods are classified into destructive or non-destructive ones. Destructive mechanical methods include deep hole-drilling method, ring core method, disk method and Sachs boring method.^{11,12)} Non-

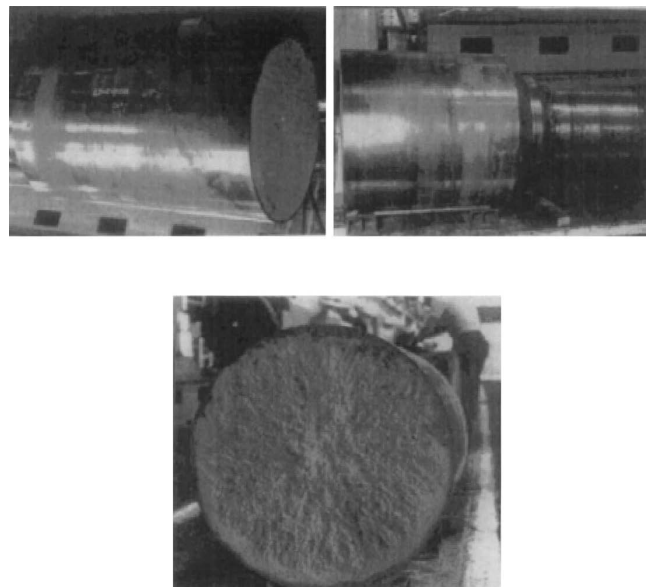


Fig. 1. An overview of the roll breakage.

destructive methods include X-ray diffraction method and Barkhausen magnetic method.^{13,14)} However, X-ray diffraction method and Barkhausen magnetic method are suitable only for measuring the surface regions and unsuitable for the interior regions of large rolls, as well as hole-drilling method and ring-core method. Deep hole-drilling method and Sachs boring method can be used for measuring the residual stress from the center to surface for very large rolls although deep hole-drilling method needs special facilities and Sachs boring method is extremely time consuming. Therefore, the disk method has been developed to predict

* Corresponding author: E-mail: noda@mech.kyutech.ac.jp
DOI: <http://dx.doi.org/10.2355/isijinternational.ISIJINT-2016-653>

the roll residual stress near the roll center, as a convenient method because of the convenience only by measuring the stress of the disk cut out from the roll.¹⁵⁻¹⁸⁾ However, attention should be paid for the relation between the roll stress and the sliced disk stress.

Since detailed studies are not available, in this paper, the accuracy of disk method will be discussed on the basis of FEM simulation. In the first place, the thermo-elastic analysis and thermo-elastic-plastic analysis will be considered to verify the relation between the cylinder stress and the sliced disk stress with single material. Next, the thermo-elastic-plastic analysis is performed to investigate the relation between the bimetallic roll residual stresses and the sliced disk residual stresses under different quenching time.

2. Disk Method and FEM Modeling

2.1. Outline of the Disk Method

To evaluate the residual stress of the cylinder, a thin disk is sliced from the original cylinder around the middle portion as shown in Fig. 2. In the first step, a disk with a thickness of about 30 mm was cut out from the cylinder. During the disk-slicing process, circumferential and axial strains at the cylinder surface were recorded with the aid of strain gauges. Since the axial stress σ_z^{Disk} on the sliced disk is completely released, the remaining residual stresses in the sliced disk are in plane stress. Then, the sliced disk stresses σ_r^{Disk} and σ_θ^{Disk} will be obtained by using X-ray diffraction method or some other ways including ring slicing and crack compliance method. Finally, the cylinder stress $\sigma_z^{Cylinder}$ will be estimated by using the sliced disk stresses σ_r^{Disk} and σ_θ^{Disk} .

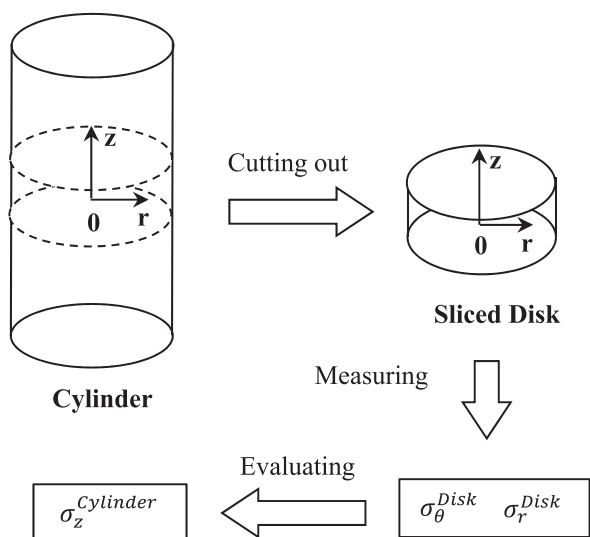


Fig. 2. Schematic diagram of the disk method.

2.2. Fundamental Equations Useful for Calculating Thermo-elastic Stresses in Circular Cylinders and Disks

To calculate thermo-elastic stresses of the cylinder and disk, the following equations are available.¹⁹⁾ When a disk is subjected to the temperature distribution $T(r)$, the thermal stresses σ_r^{Disk} and σ_θ^{Disk} are given by Eqs. (1) (2). On the other hand, the cylinder stresses $\sigma_z^{Cylinder}$, $\sigma_r^{Cylinder}$ and $\sigma_\theta^{Cylinder}$ are given by Eqs. (3) (4) (5).

$$\sigma_r^{Disk} = \alpha E \left(\frac{1}{b^2} \int_0^b T(r) r dr - \frac{1}{r^2} \int_0^r T(r) r dr \right) \dots\dots (1)$$

$$\sigma_\theta^{Disk} = \alpha E \left(-T(r) + \frac{1}{b^2} \int_0^b T(r) r dr + \frac{1}{r^2} \int_0^r T(r) r dr \right) \dots (2)$$

$$\sigma_r^{Cylinder} = \frac{\alpha E}{1-\nu} \left(\frac{1}{b^2} \int_0^b T(r) r dr - \frac{1}{r^2} \int_0^r T(r) r dr \right) = \frac{1}{1-\nu} \sigma_r^{Disk} \dots\dots\dots (3)$$

$$\sigma_\theta^{Cylinder} = \frac{\alpha E}{1-\nu} \left(\frac{1}{b^2} \int_0^b T(r) r dr + \frac{1}{r^2} \int_0^r T(r) r dr - T(r) \right) \dots (4)$$

$$= \frac{1}{1-\nu} \sigma_\theta^{Disk}$$

$$\sigma_z^{Cylinder} = \frac{\alpha E}{1-\nu} \left(\frac{2}{b^2} \int_0^b T(r) r dr - T(r) \right) = \sigma_\theta^{Cylinder} + \sigma_r^{Cylinder} \dots\dots\dots (5)$$

From the above equations, the following relation between the disk stress and the cylinder stress under the same temperature distribution can be found as Eq. (6):

$$\sigma_z^{Cylinder} = \frac{1}{1-\nu} (\sigma_r^{Disk} + \sigma_\theta^{Disk}) \dots\dots\dots (6)$$

Where, b is the cylinder or disk radius, $T(r)$ is the temperature distribution, E is the Young's modulus, α is the thermal expansion coefficient and ν is the Poisson's ratio.

2.3. FEM Analysis

Assume bimetallic rolls with diameter of 600 mm, body length of 1 800 mm and shell thickness of 75 mm, which consist of the high speed steel (HSS) as the shell material and the ductile casting iron (DCI) as the core material. Table 1 shows the chemical compositions of HSS and DCI for the common HSS bimetallic rolls, and Table 2 shows the material properties of HSS and DCI at room temperature.

Figure 3 shows the FEM model and boundary conditions for the single material roll and the bimetallic roll. Here, MSC.Marc 2012 software is used to carry out FEM analysis.

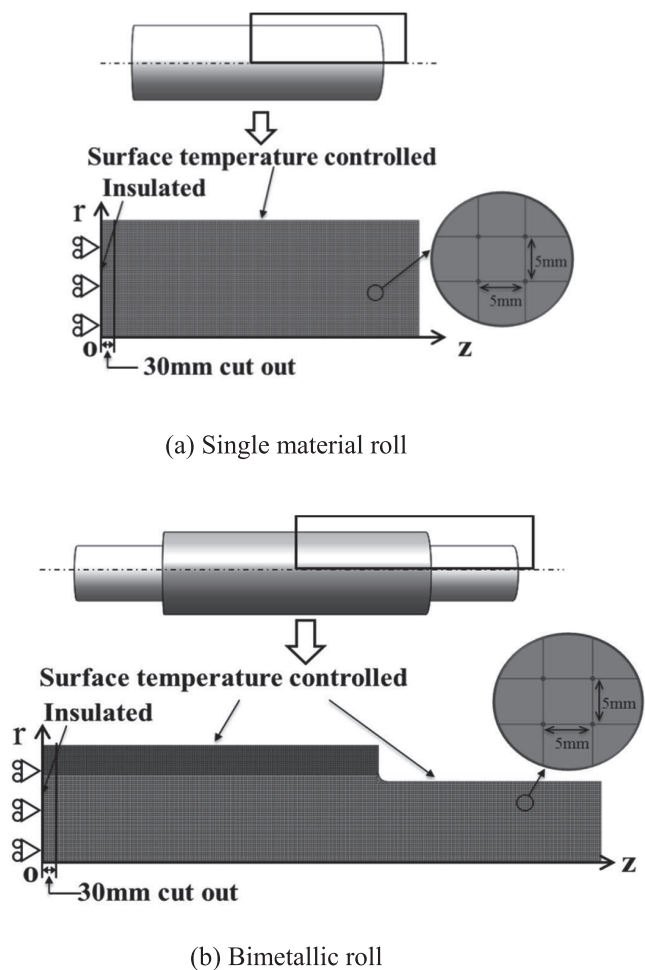
Table 1. Chemical composition of high speed steel and ductile casting iron for high speed steel roll/mass%.

Composition	C	Si	Mn	P	S	Ni	Cr	Mo	Co	V	W	Mg
HSS	1-3	<2	<1.5			<5	2-7	<10	<10	3-10	<20	<10
DCI	2.5-4	1.5-3.1		<0.1	<0.1	0.4-5	0.01-1.5	0.1-1				0.02-0.08

Table 2. Material properties of high speed steel and ductile casting iron at room temperature.

Property	HSS	DCI
0.2% proof stress [MPa]	(1 282) ^{*1}	415
Young's modulus [GPa]	233	173
Poisson's ratio	0.28	0.3
Density [kg/m ³]	7.6	7.3
Thermal expansion coefficient [K ⁻¹]	12.6 × 10 ⁻⁶	13.0 × 10 ⁻⁶
Thermal conductivity [W/(m·K)]	20.2	23.4
Specific heat [J/(kg·K)]	0.42	0.46

^{*1} Tensile strength of the shell material is indicated as the 0.2% proof stress because the deformation at break is small


Fig. 3. FEM model and boundary conditions.

A 4-node linear axisymmetric quad element with the mesh size of 5×5 mm is adopted for the transient-static simulation. The displacement boundary conditions and thermal isolation conditions are applied to $z = 0$ in Fig. 3 due to the symmetry. In this study, the temperature distribution $T(r)$ imposed to the cylinder for the thermo-elastic stress analysis and temperature is imposed to the roll surface for the thermo-elastic-plastic residual stress analysis during quenching.

In this paper, the disk with the thickness of 30 mm is cut out from the roll around the central section $z = 0$. The disk

cutting process is performed by using the deactivate element setting in the software MSC.Marc 2012. The element initial status of the sliced disk is set to activate and the rest elements are set to deactivate to simulate the disk cutting operation from the cylinder.

First, the disk method is considered for the cylinder under the temperature distribution $T(r)$ by using the DCI material properties of Young's modulus, thermal expansion and Poisson's ratio as shown in Figs. 4(a), 4(b) and 4(c).

Then, the disk method is considered for the single material roll and the bimetallic roll under the different quenching time. Before cutting the disk, the roll residual stress can be obtained through the quenching process simulation. Here, a large amount of material properties were experimentally measured under various temperatures and utilized as the input data of the quenching simulation. As shown in Figs. 4(a), 4(b), 4(c), 4(d), 4(e) and 4(f), those material properties include Young's modulus, thermal expansion coefficient, Poisson's ratio, stress-strain curves, thermal conductivity and specific heat. In Fig. 4(b), during the quenching process, the pearlite transformation occurs in the core material DCI and bainite transformation occurs in the shell material HSS. Volume expansions of core and shell accompany the phase transformations. As shown in Fig. 4(b), thermal expansion coefficient changes in 250°C – 350°C for HSS and 700°C – 720°C for DCI and are used as input data to express the volume expansions of phase transformations.

3. Thermal Stress and Residual Stress during Quenching for Single Material Roll

3.1. Thermo-elastic Stress for Cylinder and Disk

In the first place, the thermo-elastic analysis is performed for the cylinder and circular disk. Assume the cylinder center temperature $T_c = T(0) = 200^\circ\text{C}$, which often appears after the standard quenching. Assume the cylinder surface temperature $T_s = T(300) = 800^\circ\text{C}$, which may produce the surface stress $\sigma_z(300) \cong -600$ MPa often appearing at the surface after the standard quenching.^{9,10} Here, assume that all material data of DCI are depending on temperature distribution $T(r)$ as shown in Figs. 4(a), 4(b) and 4(c) for Young's modulus E , thermal expansion coefficient α and Poisson's ratio ν . Then, the thermo-elastic analysis is performed for the cylinder and the sliced disk. **Figure 5** shows the stress distribution for the cylinder stresses $\sigma_i^{\text{Cylinder}} (i = z, \theta, r)$ as the solid lines in comparison with the sliced disk stresses $\sigma_i^{\text{Disk}} (i = \theta, r)$ as the dashed lines at $z = 0$. The sliced disk stress $(\sigma_r^{\text{Disk}} + \sigma_\theta^{\text{Disk}})/(1-\nu)$ calculated from $\sigma_z^{\text{Disk}} (i = \theta, r)$ in Eq. (6) is also indicated as the dashed line. It is confirmed that the cylinder stress $\sigma_z^{\text{Cylinder}}$ coincides with the sliced disk stress $(\sigma_r^{\text{Disk}} + \sigma_\theta^{\text{Disk}})/(1-\nu)$ as shown in Fig. 5. In other words, the relation $\sigma_z^{\text{Cylinder}} = (\sigma_r^{\text{Disk}} + \sigma_\theta^{\text{Disk}})/(1-\nu)$ in Eq. (6) can be used for the thermo-elastic stress of the cylinder and sliced disk even when the material properties are depending on the temperature $T(r)$ as shown in Figs. 4(a), 4(b) and 4(c).

3.2. Residual Stress Generation Mechanism during Quenching for Single Material Roll

As shown in the above discussion, for the thermo-elastic analysis, it is found that the cylinder stress can be evaluated

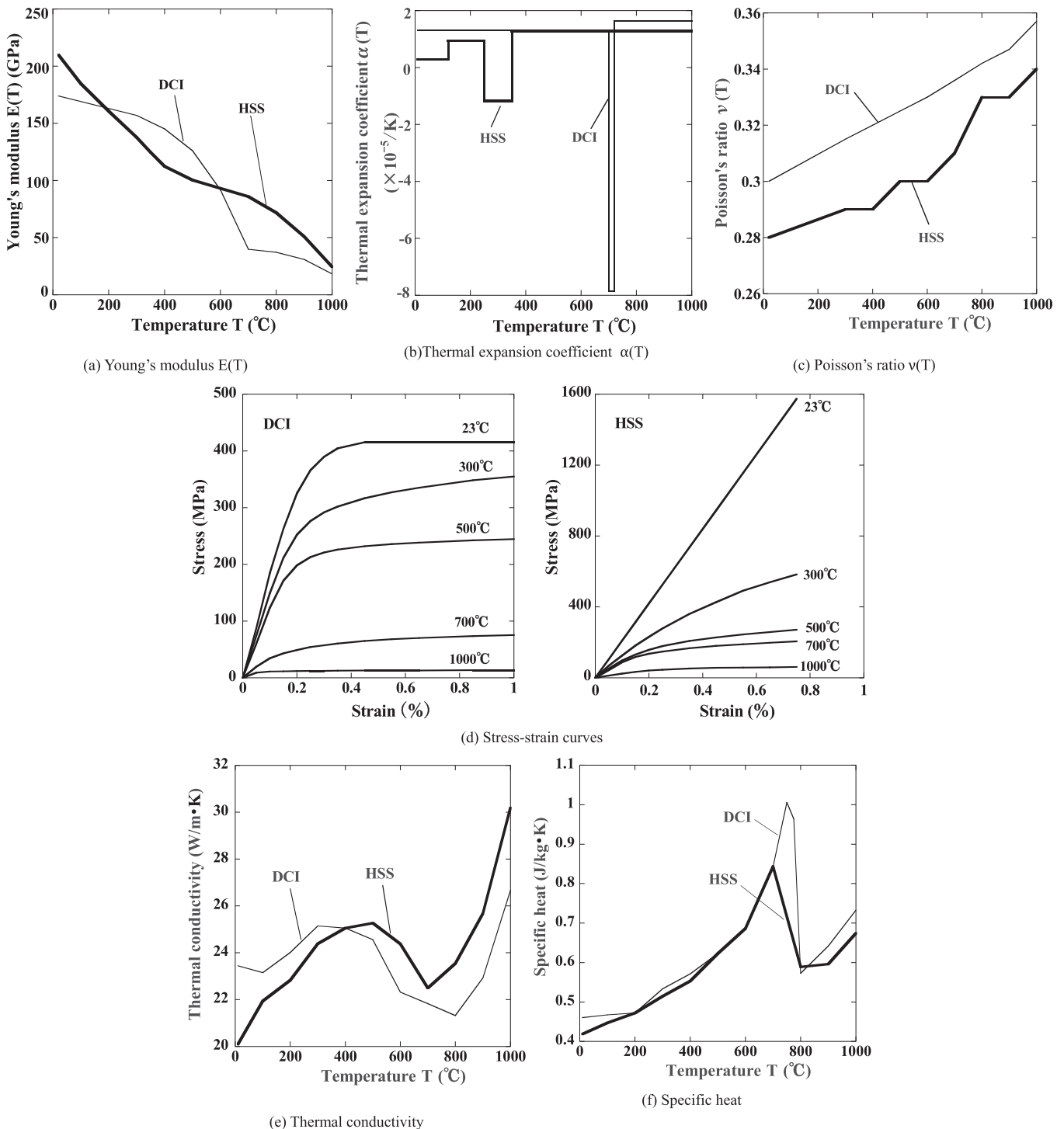


Fig. 4. Material properties dependent on temperature for high speed steel and ductile casting iron.

by the sliced disk stress. However, the residual stress of the real roll can be generated during the quenching through thermo-elastic-plastic behavior of the roll material affected by the temperature gradient and phase transformation. In this section, therefore, the residual stress generation mechanism will be explained during quenching process. In our previous studies,^{9,10)} the generation mechanism of residual stress for bimetallic roll has been discussed in detail. Here, for single material roll, the fundamental mechanism of residual stress will be discussed without considering the phase transformation.

Figure 6 shows the histories of (a) temperature T_s , T_c , (b) stress σ_z and (c) Young's modulus E , and (d) deformation

state for the single material roll during quenching process. Since FEM elastic-plastic analysis requires Young's modulus even under high temperature, 0.05% strain is focused on the stress-strain curve. Then, the Young's modulus is defined as the gradient of the line connecting the 0.05% strain point and the origin point. Figure 6(c) shows the Young's modulus E defined in this way during quenching process, which varies depending on the temperature.

The quenching process is divided into Region I (①), Region II (②) and Region III (③–⑤) classified by the dominant elastic or plastic state at the surface and center. In Region I, the yield strength of shell and core is very low due to high temperature, the stress rapidly increases and

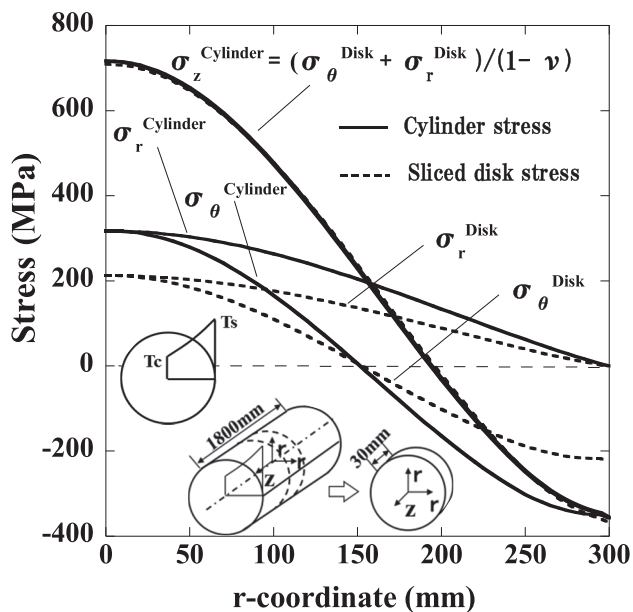


Fig. 5. Thermo-elastic stresses of the cylinder and sliced disk assuming $E = E(T)$, $\alpha = \alpha(T)$, $\nu = \nu(T)$ are depending on temperature $T(r)$ as shown in Figs. 4(a), 4(b) and 4(c) ($T_c = T(0) = 200^\circ\text{C}$, $T_s = T(300) = 800^\circ\text{C}$).

exceeds the yield stress. Therefore, the large plastic deformation occurs at both roll surface and roll center (see Fig. 6(d)①). In Region II, since the surface becomes elastic due to surface cooling, the surface Young's modulus increases with decreasing temperature although the center still keeps high temperature and plastic state (see Fig. 6(d)②). In Region III, since both surface and the center become elastic (see Fig. 6(d)③–⑤), both Young's modulus increases as the cooling continues.

In Region I, at the beginning of cooling, the surface temperature drops faster than the center temperature, leading to the temperature gradient in the r-direction (see Fig. 6(d)①). Afterwards, the roll surface shrinks relative to the center in the axial direction and results in tensile stress. In order to balance the stresses in the roll interior, the compressive stress appears in the roll center. With increasing the temperature gradient, the stress at the roll surface and center increase together continuously.

In Region II, due to continuous cooling, the roll surface turns to be elastic with increasing the Young's modulus. Meanwhile, the roll center is still plastic keeping high temperature (see Fig. 6(d)②). In this period, the thermal

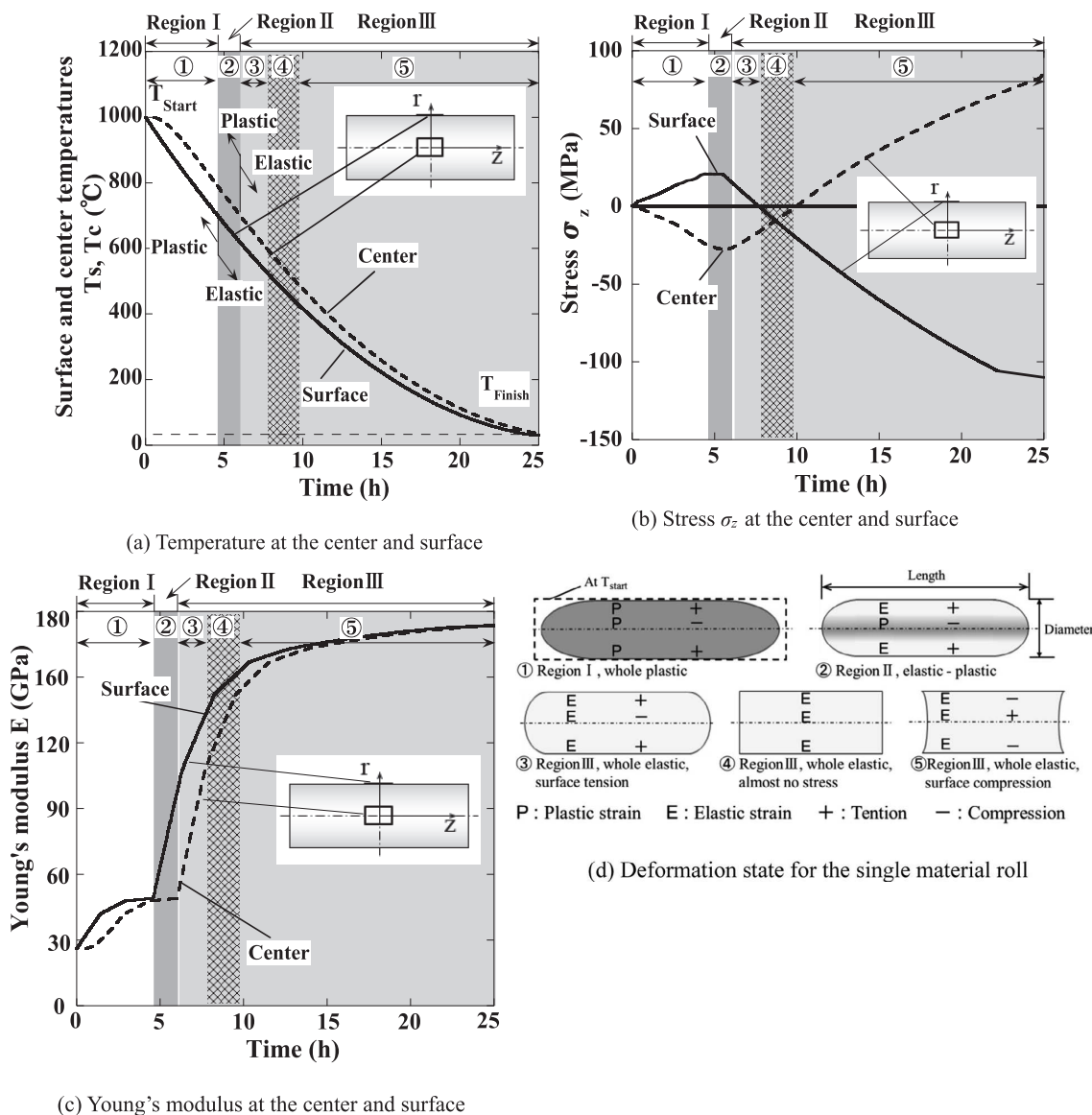


Fig. 6. Residual stress generation mechanism for the single-material roll.

contraction at the surface is restricted due to the appearing of elastic state. However, the thermal contraction rate at the center is faster than that one at the surface, causing the thermal strain differences decreasing. Finally, both the surface and center stresses reach peak values.

In Region III, thermal strain differences decreasing due to the center's thermal contraction rate is larger than surface, and both the surface and center stresses start decreasing (Fig. 6(d)③). As cooling continues, the surface thermal contraction approximately equals to the center thermal contraction, then the stresses state are interchanged (see Fig. 6(d)④). Since the center contraction is larger than that at the surface, the tensile stress increases at the roll center (see Fig. 6(d)⑤). Since Young's modulus increases in region III (see Fig. 6(c)), the compressive stresses at the roll surface increases as well as the tensile stress at the roll center. Finally, the compressive at the surface and tensile stress at the center are generated as shown in Fig. 6(b).

3.3. Residual Stress Simulation during Quenching for Single Material Roll

The thermo-elastic-plastic analysis is performed for the single material roll before and after cutting out the circular disk from the roll considering phase transformation. The residual stress is controlled by the heat treatment condition. In order to investigate the effect of heat treatment on the residual stress, different quenching time is considered. As shown in Fig. 7, several temperature changes are considered at the roll surface from 1 000°C to 100°C. Here, the different quenching time = 0.5, 1–7 h corresponds to the real roll quenching time. After quenching process, the roll is kept at 100°C until the uniform roll temperature is obtained. Here, the material properties of DCI are used as shown in Figs. 4(a)–4(f).

As shown in the above results in Fig. 5, for the thermo-elastic analysis, it is found that the ratio $\sigma_z^{Cylinder}/[(\sigma_r^{Disk} + \sigma_\theta^{Disk})/(1-\nu)] = 1$. Due to the thermo-elastic-plastic behavior, for the residual stress, the ratio $\sigma_z^{Cylinder}/[(\sigma_r^{Disk} + \sigma_\theta^{Disk})/(1-\nu)] \neq 1$. Therefore, the range of the ratio $\sigma_z^{Cylinder}/[(\sigma_r^{Disk} + \sigma_\theta^{Disk})/(1-\nu)]$ will be discussed.

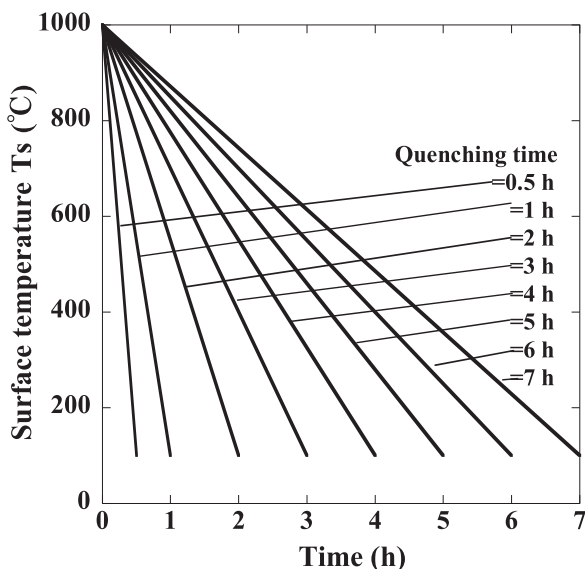


Fig. 7. Quenching time of the roll surface.

Figure 8 shows the stress ratio $\sigma_z^{Cylinder}/[(\sigma_r^{Disk} + \sigma_\theta^{Disk})/(1-\nu)]$ of the single material roll under the different quenching time. As shown in Fig. 8(a), it is seen that the ratio varies in the range of 0.73–1.49 at $r=0-100$ mm near the roll center. Here, this ratio is considered since $\sigma_z^{Cylinder}/[(\sigma_r^{Disk} + \sigma_\theta^{Disk})/(1-\nu)] \neq 1$ due to the thermo-elastic-plastic behavior. At the roll center, the stress ratio increases with increasing quenching time $t = 0.5-7$ h. It can be seen that most of the ratio $\sigma_z^{Cylinder}/[(\sigma_r^{Disk} + \sigma_\theta^{Disk})/(1-\nu)]$ at $r = 100$ mm decreases with increasing the quenching time (or decreasing quenching speed). This is because the plastic strain becomes smaller with increasing quenching time (or decreasing quenching speed). For the single material roll, it is found that the ratio $\sigma_z^{Cylinder}/[(\sigma_r^{Disk} + \sigma_\theta^{Disk})/(1-\nu)] = 0.73-1.49$ for varying the quenching time as shown in Fig. 8(a). The disk method can be used for predicting the roll residual stress by considering the above amounts of accuracy.

To clarify the effect of sliced disk thickness, FEM analysis is also performed to the disk thickness 90 mm and compared to the results of disk thickness 30 mm. When the disk thickness is 90 mm shown in Fig. 8(b), the stress ratio $\sigma_z^{Cylinder}/[(\sigma_r^{Disk} + \sigma_\theta^{Disk})/(1-\nu)]$ varies in the range of 0.78–1.41 at $r = 0-100$ mm near the roll center and becomes smaller by 6% compared with the results of the disk thickness 30 mm. It is found that the effect of disk thickness is small for the range 30–90 mm. The disk thickness results 30 mm and 90 mm in this study are useful for considering another disk thickness.

4. Residual Stress Simulation during Quenching for Bimetallic Roll

4.1. Residual Stress Simulation for Bimetallic Roll

Figure 9 shows the residual stress distribution σ_z^{Roll} of the bimetallic roll under the different quenching time in Fig. 7. It is seen that both the center tensile stress and the surface compressive stress increases with decreasing the quenching time. This is because the maximum temperature difference between the surface and center increases with decreasing the quenching time.

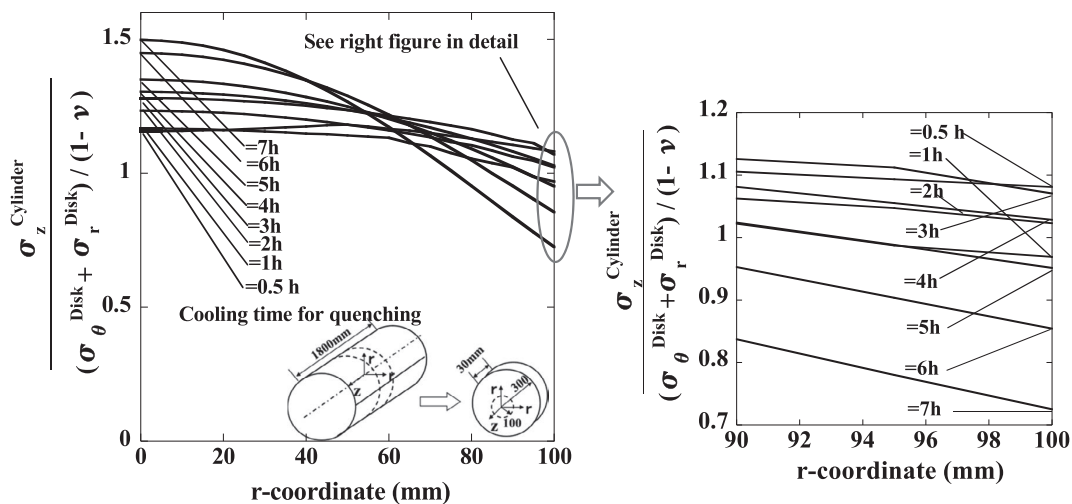
Figure 10 shows the equivalent plastic strain distribution ϵ_{eq} of the roll under the different quenching time in Fig. 7. With decreasing the quenching time, the plastic strain ϵ_{eq} becomes larger because the temperature difference between the surface and center becomes larger. It is also seen that the residual stresses in Fig. 9 are closely related to the plastic strain in Fig. 10, and both stresses at the center and surface are increasing with increasing the plastic strain.

4.2. Relation between Bimetallic Roll Stress and Sliced Disk Stress

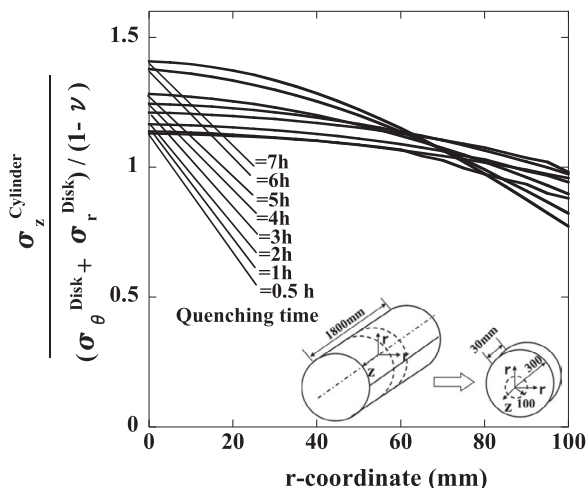
As shown in Figs. 5, 8, the relation between the roll stress $\sigma_z^{Cylinder}$ and the sliced disk stress $(\sigma_r^{Disk} + \sigma_\theta^{Disk})/(1-\nu)$ for the single material roll has been discussed. In this section, the relationship between the roll stress σ_z^{Roll} and the sliced disk stress $(\sigma_r^{Disk} + \sigma_\theta^{Disk})/(1-\nu)$ for the bimetallic roll will be discussed.

Figure 11 shows the residual stress distributions σ_r^{Disk} and σ_θ^{Disk} of the sliced disk from the bimetallic roll.

Figure 12 shows the stress ratio $\sigma_z^{Roll}/$



(a) Sliced disk thickness 30mm



(b) Sliced disk thickness 90mm

Fig. 8. Stress ratio $\sigma_z^{Cylinder} / [(\sigma_r^{Disk} + \sigma_\theta^{Disk}) / (1-\nu)]$ near the roll center of the single material roll under the different quenching time.

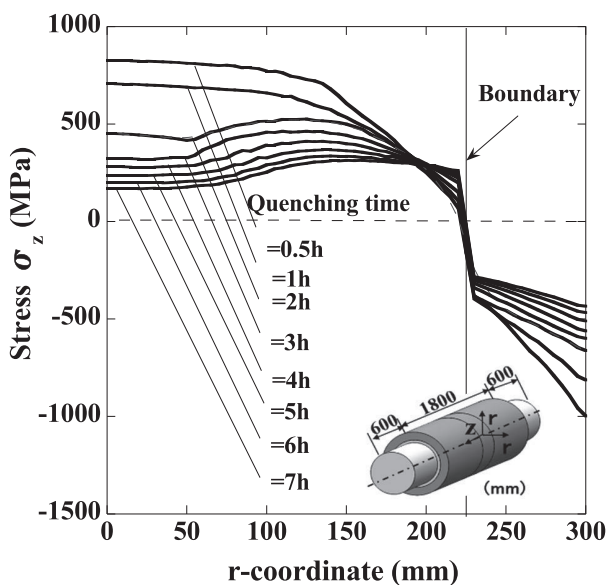


Fig. 9. Residual stress distributions σ_z^{Roll} of the bimetallic roll under the different quenching time.

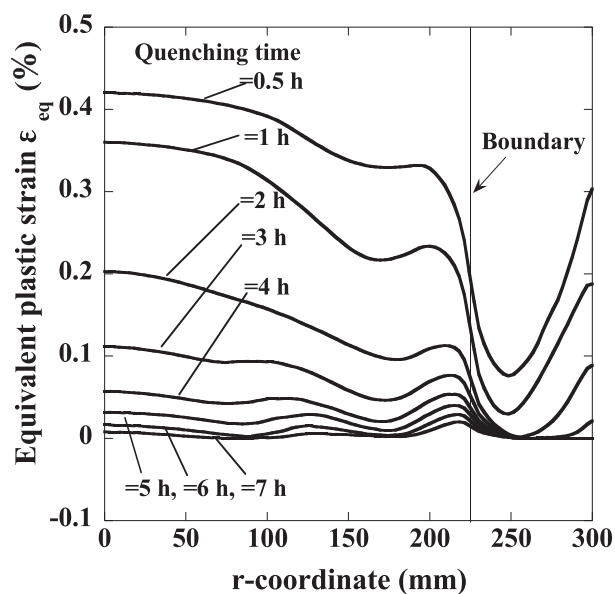


Fig. 10. Plastic strain ϵ_{eq} of the bimetallic roll under the different quenching time.

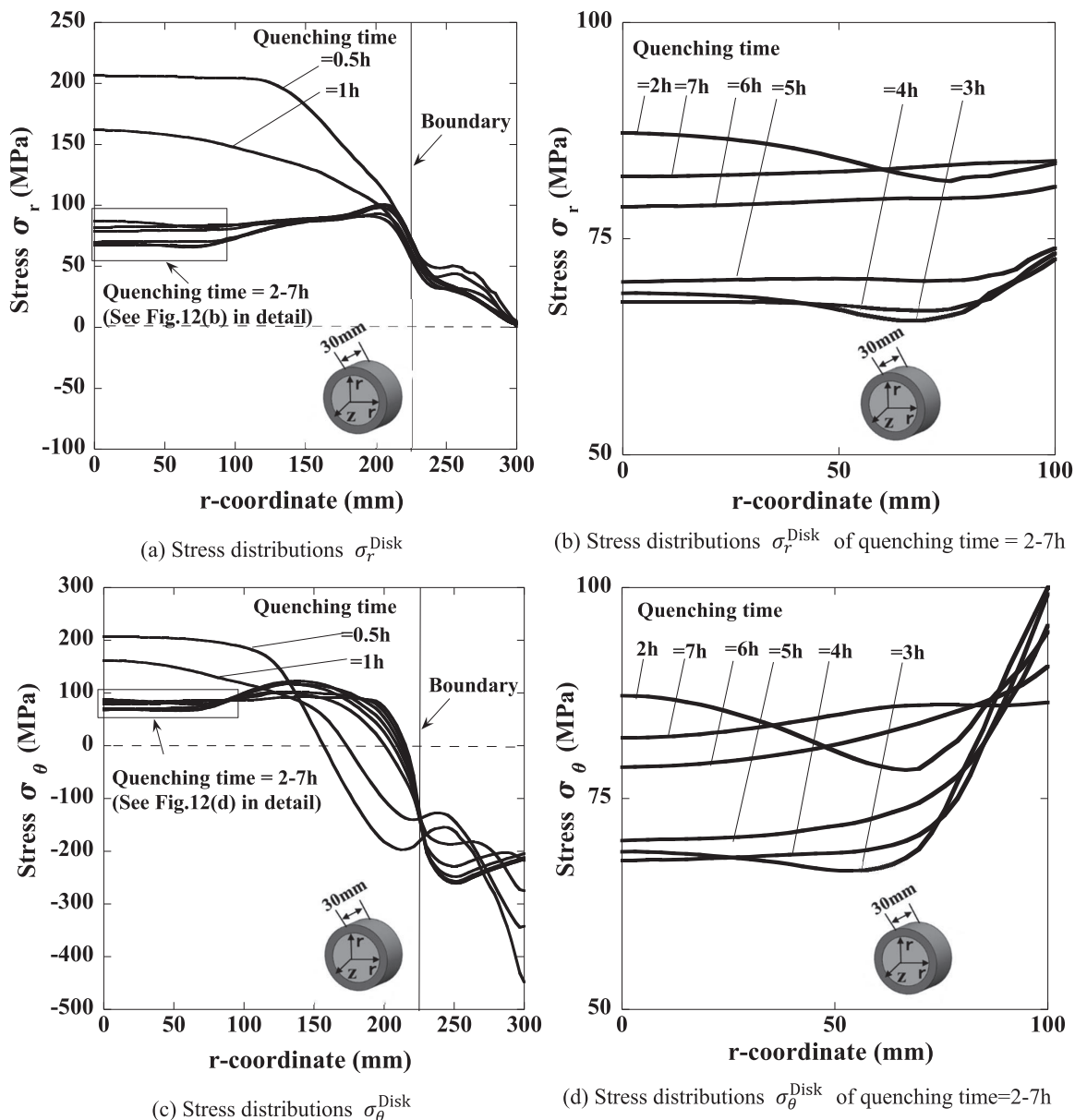


Fig. 11. Residual stress distributions σ_r^{Disk} , $\sigma_\theta^{\text{Disk}}$ of the sliced disk under the different quenching time.

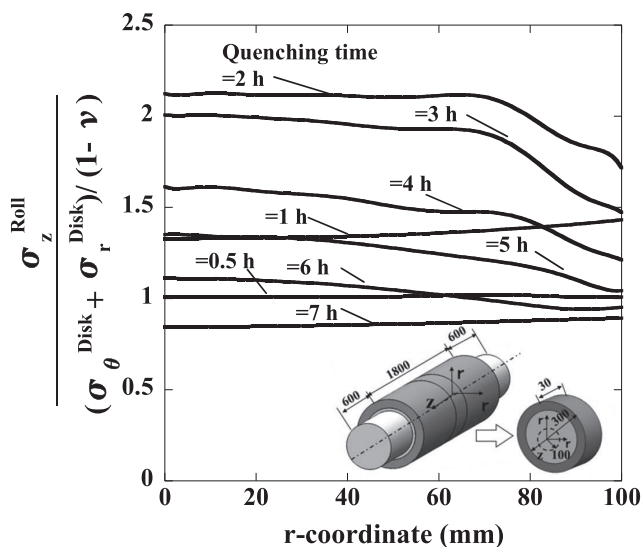


Fig. 12. Stress ratio $\sigma_z^{\text{Roll}}/[(\sigma_r^{\text{Disk}} + \sigma_\theta^{\text{Disk}})/(1-\nu)]$ near the roll center of the bimetallic roll under the different quenching time.

$[(\sigma_r^{\text{Disk}} + \sigma_\theta^{\text{Disk}})/(1-\nu)]$ of the bimetallic roll under the different quenching time. As shown in Fig. 12, the ratio is larger than 1 for the most cases and varies in the range 0.85–2.12 at $r = 0-100$ mm near the roll center. In other words, the real roll stress σ_z^{Roll} is usually larger than the sliced disk stress $(\sigma_r^{\text{Disk}} + \sigma_\theta^{\text{Disk}})/(1-\nu)$ as shown in Fig. 12. On the other hand, for the single material roll, the ratio $\sigma_z^{\text{Cylinder}}/[(\sigma_r^{\text{Disk}} + \sigma_\theta^{\text{Disk}})/(1-\nu)] = 0.73-1.49$ was obtained by varying the quenching time as shown in Fig. 8(a).

This study focused on estimating the most important residual stress σ_z by the disk method. In fact, since the actual stress σ_z is generated through the plastic deformation process, estimating σ_z is very difficult on the basis of the simple elastic theory. However, since there is no other means, the disk method can be used in a practical way to estimate the roll stress roughly. Since the disk method has been used for decades, the present discussion may be useful for roll industries.

5. Conclusions

In real work rolls, it is necessary to confirm suitable residual stress distributions. In this paper, therefore, the accuracy of disk method was investigated on the basis of FEM simulation. The relation was discussed between the bimetallic roll residual stress and the sliced disk residual stress by varying quenching time. The conclusions can be summarized in the following way.

(1) For the single material rolls it is confirmed that the thermo-elastic stress can be predicted exactly from the sliced disk from the relation $\sigma_z^{\text{Cylinder}} / [(\sigma_r^{\text{Disk}} + \sigma_\theta^{\text{Disk}}) / (1-\nu)]$ as shown in Fig. 5.

(2) For the single material rolls the thermo-elastic-plastic residual stress can be predicted by the disk method by considering the ratio $\sigma_z^{\text{Cylinder}} / [(\sigma_r^{\text{Disk}} + \sigma_\theta^{\text{Disk}}) / (1-\nu)] = 0.73\text{--}1.49$ near the roll center as shown in Fig. 8. It is confirmed that the error is insensitive to the disk thickness.

(3) For the bimetallic roll the residual stress can be predicted by the disk method considering the ratio $\sigma_z^{\text{Cylinder}} / [(\sigma_r^{\text{Disk}} + \sigma_\theta^{\text{Disk}}) / (1-\nu)] = 0.85\text{--}2.12$ near the roll center as shown in Fig. 12.

(4) The disk method has been widely used for measuring the roll residual stress. However, the accuracy of this method has not been clarified yet. In this paper, therefore, the accuracy was discussed by varying the quenching time as shown in Fig. 8 for the single material roll and shown in Fig. 12 for the bimetallic roll. The disk method can be used for predicting the roll residual stress by considering the

above amounts of accuracy.

REFERENCES

- 1) C. F. Onisa and D. C. J. Farrugia: *Int. J. Mater. Form.*, **1** (2008), 363.
- 2) A. Pérez, R. L. Corral, R. Fuentes and R. Colás: *J. Mater. Process. Technol.*, **153** (2004), 894.
- 3) D. Benasciutti: *J. Strain Anal.*, **47** (2012), 297.
- 4) D. F. Chang: *J. Mater. Process. Technol.*, **94** (1999), 45.
- 5) Y. Sano, T. Hattori and M. Haga: *ISIJ Int.*, **32** (1992), 1194.
- 6) Y. Sano and K. Kimura: *Tetsu-to-Hagané*, **73** (1987), 1154.
- 7) K. H. Schroder: *A Basic Understanding of the Mechanics of Rolling Mill Rolls*, ESW-Handbook, Eisenwerk Sulzau-Werfen, Tenneck, (2003), 71.
- 8) The European Foundry Association: *Roll Failures Manual*, Hot Mill Cast Work Rolls, CAFÉ, Roll Section, Düsseldorf, (2002), 19.
- 9) N.-A. Noda, K. Hu, Y. Sano, K. Ono and Y. Hosokawa: *Steel Res. Int.*, **87** (2016), 1478.
- 10) N.-A. Noda, K. Hu, Y. Sano, K. Ono and Y. Hosokawa: *Steel Res. Int.*, (2016), DOI: 10.1002/srin.201600165.
- 11) E. Kingston and D. J. Smith: *Ironmaking Steelmaking*, **32** (2005), 379.
- 12) X. Zhang, X. Song, L. Zhu and M. V. Li: *5th Int. Conf. on Thermal Process Modeling and Computer Simulation*, ASM International, Orlando, Florida, (2014), 6.
- 13) L. Y. Liu, J. F. Yuan and S. Y. Zhu: *Mod. Cast Iron*, **1** (1997), 21, (in Chinese).
- 14) J. Pacyna, A. Kokosza and A. S. Wojtas: *The e-Journal of Nondestructive Testing & Ultrasonics*, **4** (1999), <http://www.ndt.net/article/v04n08/wojtas/wojtas.htm>, (accessed 2016-09-10).
- 15) Y. Higashida, T. Kikuma, T. Kawanami and K. Kimura: *Tetsu-to-Hagané*, **72** (1986), 308.
- 16) M. Hinnemann, P. J. Mauk, V. Goryany, C. Zybilla and R. Braun: *Key Eng. Mater.*, **622** (2014), 949.
- 17) W. Cheng and I. Finnie: *Residual Stress Measurement and the Slitting Method*, Springer US, New York, (2007), 117.
- 18) Y. Jimbo: *J. Adv. Sci.*, **3** (1991), 157.
- 19) S. P. Timoshenko and J. N. Goodier: *Theory of Elasticity*, McGraw-Hill Book Company, New York, (1951), 408.